Spectral Compression of Narrowband Single Photons with a Resonant Cavity

Mathias A. Seidler,[1] Xi Jie Yeo,[2] Alessandro Cerè,[1] and Christian Kurtsiefer[1, 2]

[1] *Centre for Quantum Technologies, National University of Singapore, 3 Science Drive 2, Singapore 117543*
[2] *Department of Physics, National University of Singapore, 2 Science Drive 3, Singapore 117551*

(Dated: May 15, 2020)

We experimentally demonstrate a spectral compression scheme for heralded single photons with narrow spectral bandwidth around 795 nm, generated through four-wave mixing in a cloud of cold ^{87}Rb atoms. The scheme is based on an asymmetric cavity as a dispersion medium and a simple binary phase modulator, and can be, in principle, without any optical losses. We observe a compression from 20.6 MHz to less than 8 MHz, almost matching the corresponding atomic transition.

Introduction – Efficient atom-light interactions at the single quantum level is at the core of several proposals for storing, processing, and relaying quantum information [1–4]. Many of these schemes require single "flying" photons to match the spectrum of atomic transitions [5–8]. Single photons can be emitted from trapped ions [9, 10], atoms [11–13] or solid-state systems [14–16]. However, the spectral width of the generated photons may not always match the spectral width of the receving systems. Therefore, methods to engineer the photon spectrum may be required.

The simplest method for this is to passively filter the spectrum of bright broadband sources [17, 18], with a sometimes significant reduction of brightness, makeing photon-atom interaction experiments that require a high interaction rate [19, 20] difficult. More advanced methods to manipulate the spectrum of single photon sources to match that of atomic transitions include restricting the spectral mode of emitters with cavities [11, 16, 21, 22], or using electromagnetically induced transparency in atomic ensembles [23, 24] in the source mechanism altogether. Another reported approach changes the photon spectrum with a gradient echo quantum memory [25]. As spectral filtering or engineering of the photon generation mechanism may not always be possible, it would be desirable to modify the spectrum of a given photon source while maintaining the brightness.

Here, we demonstrate such a technique that compresses the spectral bandwidth of already narrowband single photons, which in principle, maintains the photon rates. The technique is based on the ideas of time-lenses invented for temporal imaging [26, 27], where the temporal and spectral characteristics of ultrafast electromagnetic pulses [28–30] are manipulated. It turns out that single photon states can be manipulated in a similar way, complementing the techniques for lossless temporal envelope manipulation of narrowband single photon states demonstrated in [31, 32].

Spectral compression of single photon wave packets is achieved in two steps: First, the wave packet is spread out in time such that the width of its envelope is compatible with a narrow spectrum; this can be done using a dispersive element that spreads out different frequency components of the wave packet in time, effectively generating a chirped wave packet. In the second step, a time-dependent phase shift is applied. This step changes the spectral energy distribution of the wave packet.

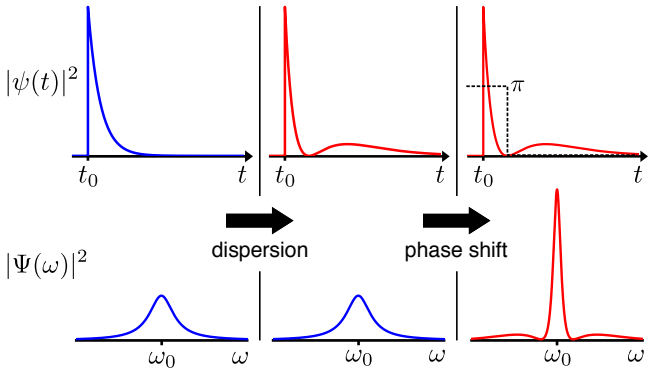

FIG. 1: Concept of spectral compression. The top row shows temporal intensity profiles $|\psi(t)|^2$ in various stages of the spectral compression, the bottom row the corresponding power spectra $|\Psi(\omega)|^2$. The initial pulse is dispersed by a cavity, leading to a new temporal shape, but an unchanged spectrum. An electro-optical modulator (EOM) manipulates the phase $\phi'(t)$ of the pulse which leads to a narrower spectrum.

Previous time-lens schemes used to spectrally compress ultrashort pulses used optical fibers or diffraction gratings as dispersive media [28–30]. For photonic wave packets interacting with single emitters like atoms or molecules, the relevant spectral bandwidth is on the order of a few MHz, which makes the use of fibers or gratings as dispersive elements impractical due to losses in the required very long fibers. We overcome this problem by using the dispersive properties of an optical cavity instead. While the dispersion in optical cavities can be much larger, the process then requires a different time-dependent phase shift in the second step to complete the spectral compression process.

Theory – To understand the spectral compression scheme, we start with an initial single photon wave packet, described by an envelope $|\psi(t)|^2$ of its intensity in time, and its corresponding power spectrum $|\Psi(\omega;\omega_0,\Gamma_p)|^2$, connected by the Fourier transform F: $\Psi(\omega) = F[\psi(t)]$. The nearly-monochromatic wave

packet shall be characterized by a central frequency ω_0 and a spectral width Γ_p. The spreading out of the wave packet in time is accomplished by reflection off an asymmetric cavity, with an input/output coupler with a low transmission, and a second high-reflective mirror, similar to the setup used in [33].

If the losses in the cavity are negligible compared to the transmission of the coupling mirror, and the cavity linewidth Γ_c and photon bandwidth Γ_p are much smaller than free spectral range of the cavity, the action of the cavity to a wave packet near its resonance ω_c can be described by a transfer function

$$C(\omega;\,\omega_c,\Gamma_c) \approx -\frac{\Gamma_c - i\,2(\omega-\omega_c)}{\Gamma_c + i\,2(\omega-\omega_c)}\,, \tag{1}$$

which modifies the incoming spectral wave packet $\Psi(\omega;\,\omega_0,\Gamma_p)$ to a new one,

$$\Psi'(\omega;\,\Delta\omega,\Gamma_c,\Gamma_p) = \Psi\,(\omega;\,\omega_0,\Gamma_p)\;C\,(\omega;\,\omega_c,\Gamma_c)\;, \tag{2}$$

where $\Delta\omega = \omega_0 - \omega_c$ is the detuning between the wave packet and the cavity resonance. For a lossless cavity, this wave packet has the same power spectrum as $\Psi(\omega)$ because $|C(\omega;\,\omega_c,\Gamma_c)|^2 = 1$. The temporal envelope of the reflected wave packet, obtained through the inverse Fourier transform F^{-1},

$$\psi'(t;\,\Delta\omega,\Gamma_c,\Gamma_p) = F^{-1}\left[\Psi'(\omega;\,\Delta\omega,\Gamma_c,\Gamma_p)\right]\,, \tag{3}$$

is now broader in time, and has acquired a time-dependent phase $\phi'(t;\,\Delta\omega,\Gamma_p,\Gamma_c)$.

Similar to Fourier-transform limited pulses, where the time-bandwidth product is minimized by a frequency-independent spectral phase, we can reduce the spectral bandwidth of the heralded single photon by removing any time-dependent phase. This is done by applying a time-dependent phase shift

$$\phi_e(t) = -\phi'(t;\;\Delta\omega,\Gamma_p,\Gamma_c)\,, \tag{4}$$

resulting in the spectrally-compressed wave packet

$$\psi''(t;\;\Delta\omega,\Gamma_p,\Gamma_c) = \psi'(t;\;\Delta\omega,\Gamma_p,\Gamma_c)\,e^{i\phi_e(t)}\,. \tag{5}$$

To quantify the compression, we compare the spectral widths before and after the compression obtained from the respective power spectrum $|\psi''(\omega;\;\Delta\omega,\Gamma_p,\Gamma_c)|^2$ obtained through a Fourier transform of Eq. (5).

We now consider the specific case of a heralded single photon emerging from an atomic cascade decay, where we intend to compress the idler photon (see inset of Fig. 2). Detection of a signal photon projects the field in the idler mode into the heralded state

$$\psi(t) = \sqrt{\Gamma_p}\,e^{-\frac{\Gamma_p}{2}(t-t_0)}\Theta(t-t_0)\,, \tag{6}$$

where t_0 and t are the detection times of the signal and idler photons, respectively. The exponential decay with

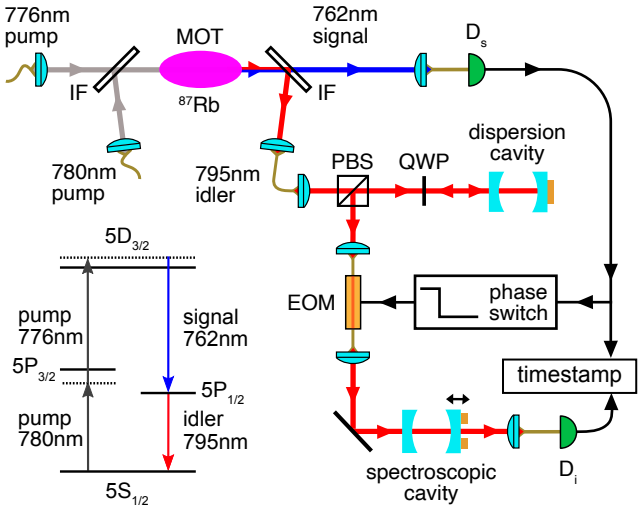

FIG. 2: Schematic setup for generation and spectral compression of heralded single photons. $D_{S,I}$: single-photon detectors, EOM: electro-optical modulator, PBS: polarizing beam splitter, QWP: quarter-wave plate, IF: interference filter. Inset: energy level scheme for four-wave mixing in ^{87}Rb.

the constant Γ_p is a characteristic of the spontaneous process, while the Heaviside step function Θ is a consequence of the well-defined time order of the cascade decay process. For simplicity, we set $t_0 = 0$.

This temporal profile corresponds to a Lorentzian power spectrum for the idler photons, and its bandwidth is described by the full-width half maximum Γ_p, which also corresponds to the spectral window containing 50% of the total pulse energy. However, the compressed spectrum $|F^{-1}\left[\psi''(t)\right]|^2$ has multiple maxima, and is distinctly different from distributions where the full-width half maximum naturally quantifies the bandwidth. Hence, we instead define bandwidth as the smallest spectral width containing 50% of the total pulse energy, as this definition of bandwidth is compatible for both a Lorentzian and a generic spectrum.

To obtain the optimal cavity parameters, we numerically minimize the bandwidth of the compressed photon spectrum. We find that the maximal compression is achieved by a resonant cavity $\Delta\omega = 0$ with a bandwidth of $\Gamma_c \approx \Gamma_p/4$. Under these conditions, the compressed single photon time envelope can be written as

$$\psi''(t) = e^{-i\phi'(t)}\,\sqrt{\Gamma_p}\,\frac{(\Gamma_p+\Gamma_c)\,e^{-\frac{\Gamma_p}{2}t} - 2\Gamma_c\,e^{-\frac{\Gamma_c}{2}t}}{\Gamma_p-\Gamma_c}\,\Theta(t)\,, \tag{7}$$

with a phase function

$$\phi'(t) = \pi\,\Theta\left(t - 2\frac{\log\left(\frac{\Gamma_p+\Gamma_c}{2\Gamma_c}\right)}{\Gamma_p-\Gamma_c}\right)\,. \tag{8}$$

This is a step function changing the phase by π, with the transition occurring at the minimum of the dispersed

photon's temporal intensity profile. The narrowest bandwidth achievable with compression based on an asymmetric cavity with this strategy is $\sim 0.3\Gamma_p$; the temporal envelopes and power spectra shown in Fig. 1 correspond to this choice.

Experiment – Details of the actual experiment are shown in Fig. 2. We generate the time-ordered photon pairs by four-wave mixing in a cold ensemble of ^{87}Rb atoms in a cascade level scheme [12]. Pump beams at 780 nm and 776 nm excite atoms from the $5S_{1/2}, F = 2$ ground level to the $5D_{3/2}, F = 3$ level via a two-photon transition. The 762 nm (signal) and 795 nm (idler) photon pairs emerge from a cascade decay back to the ground level, and are coupled to single mode fibers. Phase matching is ensured with all four modes propagating collinearly in the same direction. The two pump have a focus in the cloud with a beam waist of about 400 μm. The 780 nm pump is 55 MHz blue-detuned from the $5S_{1/2}$,F=2 to $5P_{3/2}$,F=3 transition and has an optical power of 0.25 mW. The 776 nm pump has an optical power of 11.4 mW, and is tuned such that the two-photon transition to the $5D_{3/2}$, F=3 state is 5 MHz blue-detuned. When the excited atoms decay via the $5D_{1/2}$, F=2 state back into the initial ground state, photons with a wavelength of 762 nm and 795 nm photon are emitted [12].

After suppressing residual pump light and separating signal and idler photons into different modes, we collect them into single mode fibers. The 762 nm signal photons are detected with an avalanche photo diode and herald the presence of 795 nm idler photons. The time correlation between the detection in the signal and idler modes (open circles in Fig. 3) corresponds to the envelope $|\psi(t)|^2$ of the intensity in time.

We measure the initial power spectrum of the wave packet (open circles in Fig. 4) by correlating it with a the photon rate transmitted through a Fabry-Pérot cavity (FP) with linewidth $\Gamma_{\rm FP} \approx 2\pi \times 2.6$ MHz. The transmission is recorded at different detunings of the cavity from the atomic resonance. The observed spectrum has a full width at half maximum of 20(2) MHz, wider than the atomic line width of 6 MHz due to collective emission effects in the cloud [34, 35].

The 795 nm idler photons are then coupled to the dispersion cavity, with a coupling mirror of nominal reflectivity $R_1 = 0.97$, and a high reflector with $R_2 = 0.9995$ separated by 10.1 cm, corresponding to a free spectral range of 1.48 GHz, and a measured linewidth $\Gamma_c \approx 2\pi \times 7.3$ MHz. A Pound-Drever-Hall frequency lock keeps the cavity resonant to the central frequency of the photons throughout the experiment. The measured time envelope of the single photon wave packet after dispersion is shown as filled dots in Fig. 3.

The spectral compression is completed by applying the temporal phase of Eq. (8), in the form of a phase switch synchronized to the photon passage through a fiber connected electro-optical modulator (EOM). Since the idler photon is heralded, we use the detection of the signal photon as a reference signal for triggering the phase switch after an appropriate time delay. The phase flip is applied right after the first part of the dispersed photon exits the modulator, and the second part starts to propagate through it. This timing is indicated as dashed line in Fig. 1. We finally measure the compressed photon spectrum by again recording the photon transmission rate through the Fabry-Pérot cavity, shown as filled dots in Fig. 4.

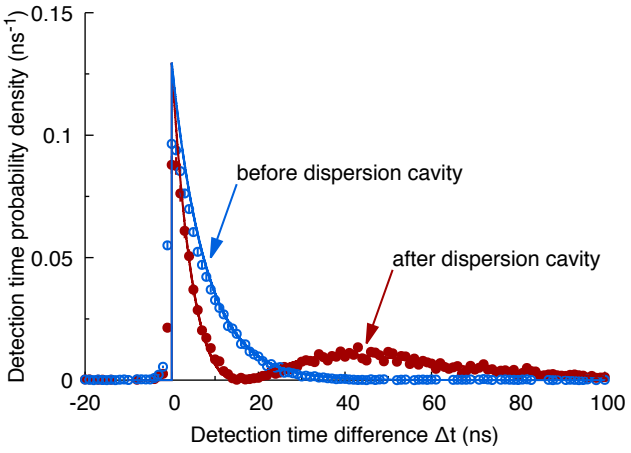

FIG. 3: Detection time distribution for the heralded photon before (open blue circles) and after (filled red dots) the dispersion cavity. We fit an exponential decay Eq. (6) to the initial time correlation (blue solid line), from which we infer the photon bandwidth Γ_p. The simulated temporal profile after the photon passed through the dispersion cavity, (red line, calculated from Eq. (2), matches our experimental data (filled dots) well.

To obtain an initial photon bandwidth Γ_p, we fit the decaying exponential term in Eq. (6) to the observed coincidence probability (open circles in Fig. 3). The solid red line in Fig. 3 corresponds to an expected temporal profile of the photon after the dispersion cavity, calculated from Eq. (7), with $\Gamma_p = 2\pi \times 20.6(2)$ MHz obtained from the fit of the initial photon shape, and the cavity linewidth $\Gamma_c \approx 2\pi \times 7.3$ MHz measured earlier. The observed temporal envelope after the dispersion cavity (full dots in Fig. 3) agrees very well with the expected profile.

The measured spectral profiles before and after compression are shown in Fig. 4. The spectrum of the uncompressed photons (open circles) exhibits a dip around the central frequency, which we attribute to reabsorption of the generated photons by the atomic cloud. We model this spectrum $S(\omega)$ by considering two processes: First, we consider the spectrum $P(\omega)$ of the photon emitted by the atomic cloud which can be obtained by the product of the spectrum of the photon produced by our FWM process $L(\omega;\Gamma_p) = \frac{2}{\pi}\frac{\Gamma_p}{4\,\omega^2+\Gamma_p^2}$ and an absorption term describing the attenuation of the photon by our atomic

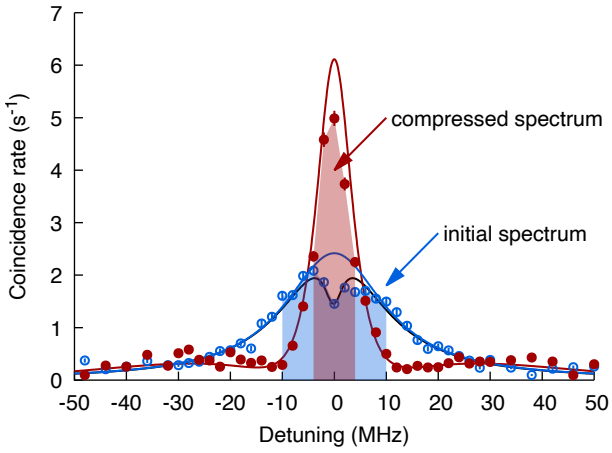

FIG. 4: Spectral profile of heralded photons before (blue) and after (red) spectral compression, obtained by measuring the photon transmission rate through the Fabry-Pérot cavity at different cavity detunings. The solid lines are calculated from Eq. (5), with Γ_p inferred from the temporal envelope measurement of the photons from the source, and Γ_c by experimentally characterizing the cavity bandwidth. Shaded areas cover 50% of the total power for each spectrum.

cloud of optical density OD

$$P(\omega; \mathrm{OD}, \Gamma_p, \Gamma_a) = A\, L(\omega; \Gamma_p)\, e^{-\mathrm{OD}\frac{\Gamma_a^2}{4\omega^2+\Gamma_a^2}}. \qquad (9)$$

The scaling factor A is used to account for the detected coincidence rate, and Γ_a is the spectral width of the absorption feature. From our fit, we extract $\Gamma_a = 2\pi \times 1.38(1.6)\,\mathrm{MHz}$, which does not correspond to the absorption linewidth of the corresponding atomic line width ($2\pi \times 5.7\,\mathrm{MHz}$) of the $5S_{1/2} \rightarrow 5P_{1/2}$ transition. Further work is necessary to understand this observation. The photon bandwidth $\Gamma_p = 2\pi \times 20.6(2)\,\mathrm{MHz}$ was determined from the photon coincidence time correlation (Fig. 3). Second, we consider the effect of the Fabry-Pérot cavity used to sample the spectral profile by convolution the above result with $L'(\omega; \Gamma_{\mathrm{FP}}) = \frac{\Gamma_{\mathrm{FP}}^2}{4\,\omega^2+\Gamma_{\mathrm{FP}}^2}$ to model the observed spectrum:

$$S(\omega) = (P * L')(\omega). \qquad (10)$$

We fit the model $S(\omega)$ (Fig. 4, black line) to the experimental data corresponding to the spectral profile of the photon without sending a signal to the EOM (Fig. setup) used to compress the photon. The model, without considering the attenuation of the atomic cloud, is given by $(A\,L * L')(\omega)$ (Fig. 4, blue line). This is provided as a reference for a Fourier-transform limited photon with an exponentially decaying envelope, as emitted by a single atom - the scenario examined in the theory section.

To apply the analysis in the theory section for predicting the spectrum of the compressed photon, we first rescale the power spectrum $|\Psi''(\omega)|^2$, calculated from Eq. (7), with A, which was extracted from the previous fit. Then, we convolve this spectrum with $L'(\omega; \Gamma_{\mathrm{FP}})$ to obtain the expected compressed photon spectrum $(A\,|\Psi''|^2 * L')(\omega)$. Figure 4 (red line) shows the modeled power spectrum slightly deviating from the measured result (red dots), exhibiting a lower peak coincidence rate where an absorption dip occurs in the uncompressed photon spectrum (blue dots). We attribute this difference to the fact that our model does not fully account for the effects imposed by the atomic cloud.

Discussion – By definition, spectral compression reduces the width of a spectral distribution, resulting in an increased photon rate/intensity at the central frequency. In our experiment, we find a bandwidth of 20(2) MHz for the initial, and 8(2) MHz for the compressed photon. This almost matches the natural D transition linewidth of 6 MHz in ^{87}Rb. The maximal photon transmission through the spectroscopic cavity is increased by a factor of 2.39(4), indicating a successful spectral compression of narrowband photons.

The compressions mechanism is, in principle, lossless since both cavity and phase modulators can have arbitrarily low losses. In our experiment, we incur a total photon loss of about 79% due to the compression optics. We measure an optical transmission of 60% through the dispersion optics (PBS, QWP, dispersion cavity, fiber coupling), and 35.7% through the fiber-based EOM. The photon loss can be significantly reduced by replacing the fiber-based EOM with a free-space EOM.

The optimal spectral compression of a photon with bandwidth Γ_p in the cavity-based scheme is achieved if the dispersion cavity has a bandwidth of $0.25\,\Gamma_p$. Since the amount of spectral compression is limited by the dispersion mechanism, dispersion engineering of structured dielectric media [36–38] or multiple combined optical cavities may allow to further increase the spectral compression. This method is not limited to the atomic system in our experiment – it can be adapted to a wide range of wavelengths and spectral widths, and therefore even allow to match the spectral properties to different types of quantum systems e.g. in a hybrid quantum network [39].

We thank Adrian Nugraha Utama for useful discussions on the theoretical modeling and Jianwei Lee for his valuable input while writing this script. This work was supported by the Ministry of Education in Singapore.

[1] J. I. Cirac, P. Zoller, H. J. Kimble, and H. Mabuchi, Phys. Rev. Lett. **78**, 3221 (1997).
[2] H.-J. Briegel, W. Dür, J. I. Cirac, and P. Zoller, Phys. Rev. Lett. **81**, 5932 (1998).
[3] E. Waks and C. Monroe, Phys. Rev. A **80**, 062330 (2009).
[4] H. J. Kimble, Nature **453**, 1023 (2008).
[5] T. Wilk, S. C. Webster, A. Kuhn, and G. Rempe, Science **317**, 488 (2007).

[6] K. Hammerer, A. S. Sørensen, and E. S. Polzik, Rev. Mod. Phys. **82**, 1041 (2010).
[7] M. D. Lukin, Rev. Mod. Phys. **75**, 457 (2003).
[8] M. Steiner, V. Leong, M. A. Seidler, A. Cerè, and C. Kurtsiefer, Opt. Express **25**, 6294 (2017).
[9] M. Keller, B. Lange, K. Hayasaka, W. Lange, and H. Walther, Nature **431**, 1075 (2004).
[10] M. Almendros, J. Huwer, N. Piro, F. Rohde, C. Schuck, M. Hennrich, F. Dubin, and J. Eschner, Phys. Rev. Lett. **103**, 213601 (2009).
[11] A. Kuhn, M. Hennrich, and G. Rempe, Phys. Rev. Lett. **89**, 067901 (2002).
[12] B. Srivathsan, G. K. Gulati, B. Chng, G. Maslennikov, D. N. Matsukevich, and C. Kurtsiefer, Phys. Rev. Lett. **111**, 123602 (2013).
[13] J. Park, H. Kim, and H. S. Moon, Phys. Rev. Lett. **122**, 143601 (2019).
[14] C. Kurtsiefer, S. Mayer, P. Zarda, and H. Weinfurter, Phys. Rev. Lett. **85**, 290 (2000).
[15] P. Michler, A. Kiraz, C. Becher, W. Schoenfeld, P. Petroff, L. Zhang, E. Hu, and A. Imamoglu, Science **290**, 2282 (2000).
[16] E. Moreau, I. Robert, J. Gérard, I. Abram, L. Manin, and V. Thierry-Mieg, Appl. Phys. Lett. **79**, 2865 (2001).
[17] E. Meyer-Scott, N. Montaut, J. Tiedau, L. Sansoni, H. Herrmann, T. J. Bartley, and C. Silberhorn, Phys. Rev. A **95**, 1 (2017).
[18] C. Schuck, F. Rohde, N. Piro, M. Almendros, J. Huwer, M. W. Mitchell, M. Hennrich, A. Haase, F. Dubin, and J. Eschner, Phys. Rev. A **81**, 1 (2010).
[19] L.-M. Duan, M. D. Lukin, J. I. Cirac, and P. Zoller, Nature **414**, 413 (2001).
[20] B. B. Blinov, D. L. Moehring, L.-M. Duan, and C. Monroe, Nature **428**, 153 (2004).
[21] J. McKeever, A. Boca, A. D. Boozer, R. Miller, J. R. Buck, A. Kuzmich, and H. J. Kimble, Science **303**, 1992 (2004).
[22] F. Wolfgramm, X. Xing, A. Cerè, A. Predojević, A. M. Steinberg, and M. W. Mitchell, Opt. Express **16**, 18145 (2008).
[23] M. Eisaman, A. André, F. Massou, M. Fleischhauer, A. Zibrov, and M. Lukin, Nature **438**, 837 (2005).
[24] L. Zhu, X. Guo, C. Shu, H. Jeong, and S. Du, Appl. Phys. Lett. **110**, 161101 (2017).
[25] B. Buchler, M. Hosseini, G. Hétet, B. Sparkes, and P. K. Lam, Opt. Lett. **35**, 1091 (2010).
[26] B. H. Kolner and M. Nazarathy, Opt. Lett. **14**, 630 (1989).
[27] B. H. Kolner, IEEE J. Quantum Electron. **30**, 1951 (1994).
[28] J. Lavoie, J. M. Donohue, L. G. Wright, A. Fedrizzi, and K. J. Resch, Nat. Photonics **7**, 363 (2013).
[29] M. Karpiński, M. Jachura, L. J. Wright, and B. J. Smith, Nat. Photonics **11**, 53 (2016).
[30] Y. Li, T. Xiang, Y. Nie, M. Sang, and X. Chen, Sci. Rep. **7**, 43494 (2017).
[31] B. Srivathsan, G. K. Gulati, A. Cerè, B. Chng, and C. Kurtsiefer, Phys. Rev. Lett. **113**, 1 (2014).
[32] O. Morin, M. Körber, S. Langenfeld, and G. Rempe, Phys. Rev. Lett. **123**, 133602 (2019).
[33] B. Srivathsan, G. K. Gulati, A. Cerè, B. Chng, and C. Kurtsiefer, Phys. Rev. Lett. **113**, 163601 (2014).
[34] H. H. Jen, Phys. Rev. A **85**, 013835 (2012).
[35] A. Cerè, B. Srivathsan, G. K. Gulati, B. Chng, and C. Kurtsiefer, Phys. Rev. A **98**, 023835 (2018).
[36] E. Istrate and E. H. Sargent, Rev. Mod. Phys. **78**, 455 (2006).
[37] X. Li, M. Pu, X. Ma, Y. Guo, P. Gao, and X. Luo, J. Phys. D: Appl. Phys. **51**, 054002 (2018).
[38] J. D. Joannopoulos, S. G. Johnson, J. N. Winn, and R. D. Meade, *Photonic Crystals: Molding the Flow of Light*, 2nd ed. (Princeton University Press, Princeton, NJ, USA, 2008).
[39] G. Kurizki, P. Bertet, Y. Kubo, K. Mølmer, D. Petrosyan, P. Rabl, and J. Schmiedmayer, Proc. Natl. Acad. Sci. U.S.A **112**, 3866 (2015).